Author/s:
Mak, JYW;Rivero, RJD;Hoang, HN;Lim, XY;Deng, J;McWilliam, HEG;Villadangos, JA;McCluskey, J;Corbett, AJ;Fairlie, DP

Title:
Potent Immunomodulators Developed from an Unstable Bacterial Metabolite of Vitamin B2 Biosynthesis

Date:
2024-07-29

Citation:
Mak, J. Y. W., Rivero, R. J. D., Hoang, H. N., Lim, X. Y., Deng, J., McWilliam, H. E. G., Villadangos, J. A., McCluskey, J., Corbett, A. J. & Fairlie, D. P. (2024). Potent Immunomodulators Developed from an Unstable Bacterial Metabolite of Vitamin B2 Biosynthesis. Angewandte Chemie International Edition, 63 (31), https://doi.org/10.1002/anie.202400632.

Persistent Link:
https://hdl.handle.net/11343/351049

How to cite: *Angew. Chem. Int. Ed.* **2024**, *63*, e202400632
doi.org/10.1002/anie.202400632

Covalent Ligands

Potent Immunomodulators Developed from an Unstable Bacterial Metabolite of Vitamin B2 Biosynthesis

Jeffrey Y. W. Mak, Ryan J. D. Rivero[+], Huy N. Hoang[+], Xin Yi Lim[+], Jieru Deng, Hamish E. G. McWilliam, Jose A. Villadangos, James McCluskey, Alexandra J. Corbett, and David P. Fairlie**

Abstract: Bacterial synthesis of vitamin B2 generates a by-product, 5-(2-oxopropylideneamino)-D-ribityl-aminouracil (5-OP-RU), with potent immunological properties in mammals, but it is rapidly degraded in water. This natural product covalently bonds to the key immunological protein MR1 in the endoplasmic reticulum of antigen presenting cells (APCs), enabling MR1 refolding and trafficking to the cell surface, where it interacts with T cell receptors (TCRs) on mucosal associated invariant T lymphocytes (MAIT cells), activating their immunological and antimicrobial properties. Here, we strategically modify this natural product to understand the molecular basis of its recognition by MR1. This culminated in the discovery of new water-stable compounds with extremely powerful and distinctive immunological functions. We report their capacity to bind MR1 inside APCs, triggering its expression on the cell surface (EC_{50} 17 nM), and their potent activation (EC_{50} 56 pM) or inhibition (IC_{50} 80 nM) of interacting MAIT cells. We further derivatize compounds with diazirine-alkyne, biotin, or fluorophore (Cy5 or AF647) labels for detecting, monitoring, and studying cellular MR1. Computer modeling casts new light on the molecular mechanism of activation, revealing that potent activators are first captured in a tyrosine- and serine-lined cleft in MR1 via specific pi-interactions and H-bonds, before more tightly attaching via a covalent bond to Lys43 in MR1. This chemical study advances our molecular understanding of how bacterial metabolites are captured by MR1, influence cell surface expression of MR1, interact with T cells to induce immunity, and offers novel clues for developing new vaccine adjuvants, immunotherapeutics, and anticancer drugs.

Introduction

Peptides and glycolipids have long been known to be ligands (antigens) that activate T lymphocytes (T cells).[1] However, we discovered that uracil derivatives can also activate T cells, specifically mucosal associated invariant T cells (MAIT cells).[2,3] These cells are abundant in the mucosa[4] and peripheral blood and are now recognized as being important for antimicrobial defense, tissue repair, and protection against cancer.[5] They are activated by bacterial metabolites derived from 5-amino-6-D-ribityl-aminouracil, 5-A-RU (**1**, Figure 1), a key biosynthetic precursor to vitamin B2 (**2**).[2] For example, condensation of **1** with glycolysis metabolite methylglyoxal (**3**) creates the novel and highly potent heterocyclic antigen 5-(2-oxopropylideneamino)-D-ribitylaminouracil (5-OP-RU, **4**) (Figure 1).[3]

The bacterial natural product 5-OP-RU (**4**) enters mammalian cells and binds to the antigen presenting protein MR1 in the endoplasmic reticulum (Figure 2a).[6] Its binding induces refolding of MR1, triggering translocation of the MR1-bound complex of 5-OP-RU (**4**) to the surface of the antigen presenting cell (APC).[6] There, this complex engages a T cell receptor (MAIT TCR) on the surface of MAIT cells, resulting in activation that can be detected by

[*] Dr. J. Y. W. Mak, R. J. D. Rivero,[+] Dr. H. N. Hoang,[+] Prof. Dr. D. P. Fairlie
Centre for Chemistry and Drug Discovery and ARC Centre of Excellence for Innovations in Peptide and Protein Science
Institute for Molecular Bioscience, The University of Queensland
Brisbane, Queensland, 4072, Australia
E-mail: j.mak@uq.edu.au
d.fairlie@uq.edu.au

X. Y. Lim,[+] Dr. J. Deng, Dr. H. E. G. McWilliam, Prof. Dr. J. A. Villadangos, Prof. Dr. J. McCluskey, Assoc. Prof. Dr. A. J. Corbett
Department of Microbiology and Immunology
The University of Melbourne, at the Peter Doherty Institute for Infection and Immunity
Melbourne, Victoria 3000, Australia

Prof. Dr. J. A. Villadangos
Department of Biochemistry and Pharmacology
Bio21 Molecular Science and Biotechnology Institute, The University of Melbourne
Parkville, Victoria 3010, Australia

[+] These authors contributed equally.

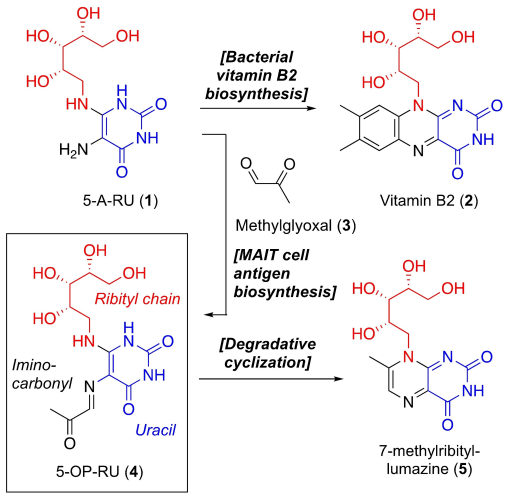

Figure 1. Intermediate **1** from bacterial synthesis of vitamin B2 (**2**) condenses with glycolysis metabolite (**3**) to form a transient MAIT cell antigen 5-OP-RU (**4**), which rapidly degrades to lumazine **5**.[3]

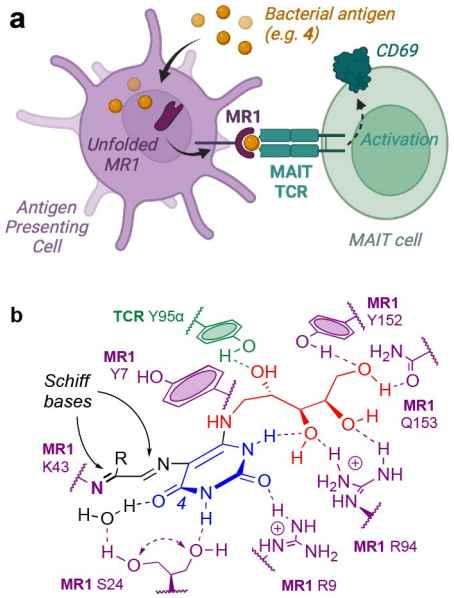

Figure 2. Binding of 5-OP-RU (**4**) to MR1 protein and activation of MAIT cells.[5] (a) Bacterial antigens (orange) enter antigen presenting cells (APC, purple), then bind to protein MR1 in the endoplasmic reticulum. The MR1-antigen complex is translocated to the APC surface, where it interacts with the T cell receptor (TCR, green) on MAIT cells (green). (b) Interactions of **4** with MR1 (purple) and MAIT TCR (green) from a crystal structure of the ternary complex.[3]

protein surface markers like CD69 (Figure 2a).[5] A crystal structure revealed that the ribityl chain of **4** interacts at the MR1-TCR interface, while the uracil and iminocarbonyl groups bind to MR1. The iminocarbonyl covalently forms an imine (Schiff base) with the sidechain of lysine-43 (K43) of MR1 (Figure 2b),[3] stabilizing the ligand and inducing MR1 refolding.

The natural product 5-OP-RU (**4**) has been used to characterize roles for MR1 and MAIT cells in mammalian health and disease.[7] The abundance of MAIT cells relative to other T cells supports their importance in immunity,[8] and MR1 is emerging as a potential drug target.[7,8b,9] 5-OP-RU (**4**) promotes MAIT cell development in the thymus[10] and imprints MAIT cells in early life,[11] confers MAIT cells with an ability to protect against infections,[12,13] promotes wound healing,[11,14] kills myeloma cells in vitro,[15] and protects against melanoma in mice.[16] Dysregulated MAIT cell activation has been linked to gastritis,[17] asthma,[18] and inflammatory bowel disease.[19]

Despite these advances, MAIT cell immunology is still hampered by a lack of stable and effective chemical tools.[9b] While 5-OP-RU (**4**) is a potent immunostimulant, its utility is limited by instability in water due to rapid cyclization or imine hydrolysis to form lumazine **5**, which is orders of magnitude less potent.[20] Structural requirements for MR1-ligand binding remain to be fully elucidated, no potent inhibitors of MAIT cell activation are known, and very few chemical tools are available to probe the properties of MAIT cells. Here, the bacterial metabolite 5-OP-RU (**4**) has been strategically modified to study the molecular basis of its biological activity. This led to the development of water-stable compounds with stronger MR1 binding and upregulation to the APC surface, more potent MAIT cell activation or inhibition, and better tools for detecting and modulating MR1 protein and MAIT cell functions. These new stable compounds provide new insights to MR1-binding requirements, to the molecular mechanism of ligand capture by MR1, and to how to tailor ligands for distinctively different immunological properties and uses in interrogating MR1 and MAIT cell immunology.

Results and Discussion

Molecular Requirements for MR1 Upregulation to the Cell Surface

The importance of each ribityl hydroxyl group in 5-OP-RU (**4**) for upregulated MR1 expression on the cell surface and MAIT cell activation has been reported previously.[21] Here, we removed the MR1-binding ribityl chain to assess contributions from the imine and uracil components of **4** to MR1 upregulation. To potentially increase aqueous stability, we also replaced the exocyclic nitrogen atoms of the uracil and the iminocarbonyl with carbon atoms.[20] Compound **10** was synthesized from 6-methyluracil (**6a**) via hydroxymethylation (to **7a**, 70 %), ceric ammonium nitrate (CAN) oxidation (to **8a**, 56 %), and elaboration with stabilized ylide **9a**[22] (Scheme 1). Compound **10** was much more water-stable (>99 % over 24 h) than 5-OP-RU (**4**) ($t_{1/2}$~88 min) at 37 °C, pH 7.4 (Figure 3), since it lacks the imine and amine nitrogens of **4** known to promote degradation,[20] making it useful for studying how modification affects potency, and as a scaffold to support the construction of other more complex ligands.

When ligands bind to MR1 in cells via an imine bond with K43, they induce refolding of MR1 that enables translocation of the MR1-ligand complex to the cell surface

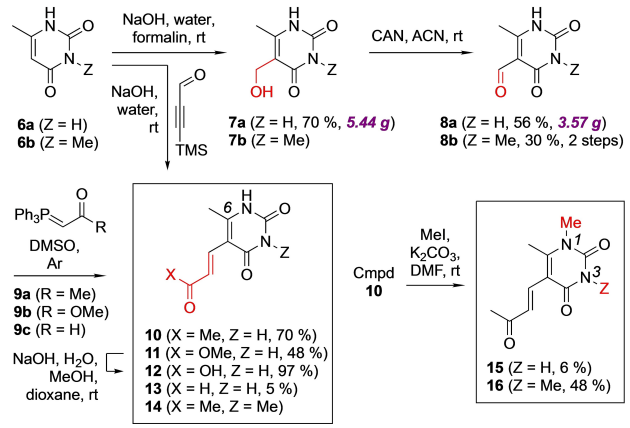

Scheme 1. Synthesis of MR1-binding analogues of **4**.

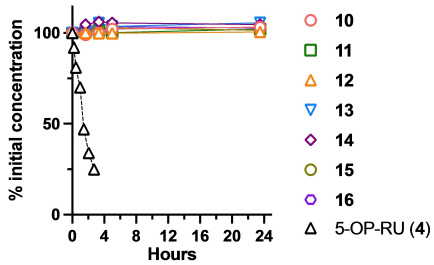

Figure 3. Stability of **10**–**16** (0.1 mM) in phosphate buffered saline (37 °C, pH 7.4), relative to 5-OP-RU (**4**).[20]

(Figure 2a). MR1 binding was inferred here using an established assay[3] that measures increased MR1 surface expression on class I reduced (C1R) cells overexpressing MR1 (C1R.MR1 cells) (Figure 4). Compound **10** was found here to upregulate MR1 expression (EC_{50} 17 nM) more potently over 16 h than the much less stable 5-OP-RU (**4**) (EC_{50} 1.7 μM). Next, we synthesized analogues of **10** to investigate contributions of the sidechain carbonyl and uracil nitrogen components to MR1 binding. To obtain carbonyl analogues **11**–**13**, elaboration of aldehyde **8a** with stabilized ylide **9b** gave the corresponding ester, and its carboxylic acid after saponification (**11** and **12**, Scheme 1). For aldehyde **13**, since intermediate **8a** polymerized with ylide **9c**, we directly alkenylated[20] **6a** to give **13** (5 % yield, attributable to the hydration and inactivation of trimethylsilylpropynal in water). To obtain the *N*-methylated uracil analogues (**14**–**16**), we next treated **10** with methyl iodide to give **15** and **16**, and then used *N*-methyluracil **6b**[23] to access analogue **14** via **7b** and **8b**.

Analogues **10**–**16** were all very water stable (pH 7.4, 37 °C, 24 h, Figure 3, Figure S1). Unlike 5-OP-RU (**4**) and **10**, ester **11** and acid **12** can only make weak hydrogen bonds or electrostatic interactions with MR1 lysine-43 (K43, Figure 2b) and did not upregulate MR1 (Figure 4). Conversely, aldehyde **13** (EC_{50} 2.1 nM) was a potent MR1 upregulator, 10-fold more than ketone **10** (EC_{50} 17 nM) and 800-fold more potent than 5-OP-RU (**4**) (EC_{50} 1.7 μM) after 16 h (Figure 4). This highlights the importance of the covalent imine bond, formed between a reactive carbonyl group and the K43 residue of MR1 (Figure 2b), for MR1 binding and upregulation to the cell surface (Figure 4).

Previous studies using K43 mutagenesis showed the importance of imine formation for MR1 refolding,[6] but here we directly modified the ligand to show that charge neutralization through imine formation, rather than perturbing K43 interactions within the MR1 protein, is responsible for MR1 upregulation. Notably, compounds **10** and **13** were not Michael acceptors like the control compound crotonaldehyde (Figure 5), instead being resistant at pH 7.4 to reaction for example with glutathione.[24]

N-methylated analogue **14** (EC_{50} 4.0 μM) was 200-fold less potent than **10** in upregulating MR1, consistent with it being unable to form a hydrogen bond with serine-24 (S24) of MR1 (Figure 2b). Methylation of the NH at position 1, which does not directly hydrogen bond to MR1, also reduced potency (**15**, EC_{50} 3.2 μM), with double *N*-methylation (**16**) abolishing this activity (>100 μM). Consistent with previous studies,[7,25] systematic uracil *N*-methylation showed that MR1 can accommodate modified uracils, but is also sensitive to even small structural changes.

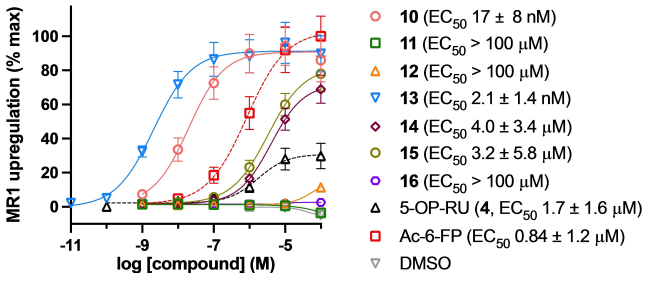

Figure 4. Dose-dependent upregulation of MR1 expression on the surface of C1R.MR1 cells after 16 h exposure to **10**–**16**. Upregulation by acetyl 6-formylpterin (Ac-6-FP, 0.1 mM) defined as 100 %. Each data point represents mean ± SEM ($n = 3$). EC_{50} values shown ± SEM.

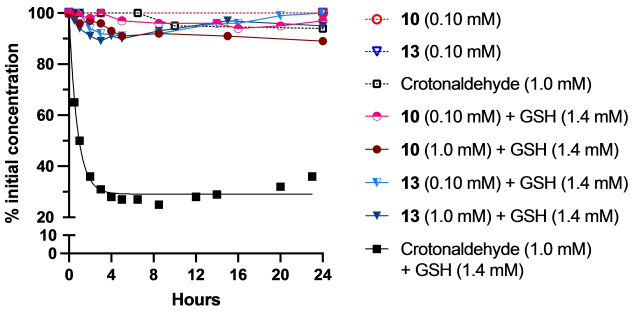

Figure 5. Degradation of **10** (○) and **13** (▽) versus crotonaldehyde (■) in the presence of glutathione (GSH) in phosphate buffered saline (pH 7.4) at room temperature. The degradation of crotonaldehyde with glutathione was fitted to a one phase decay curve.

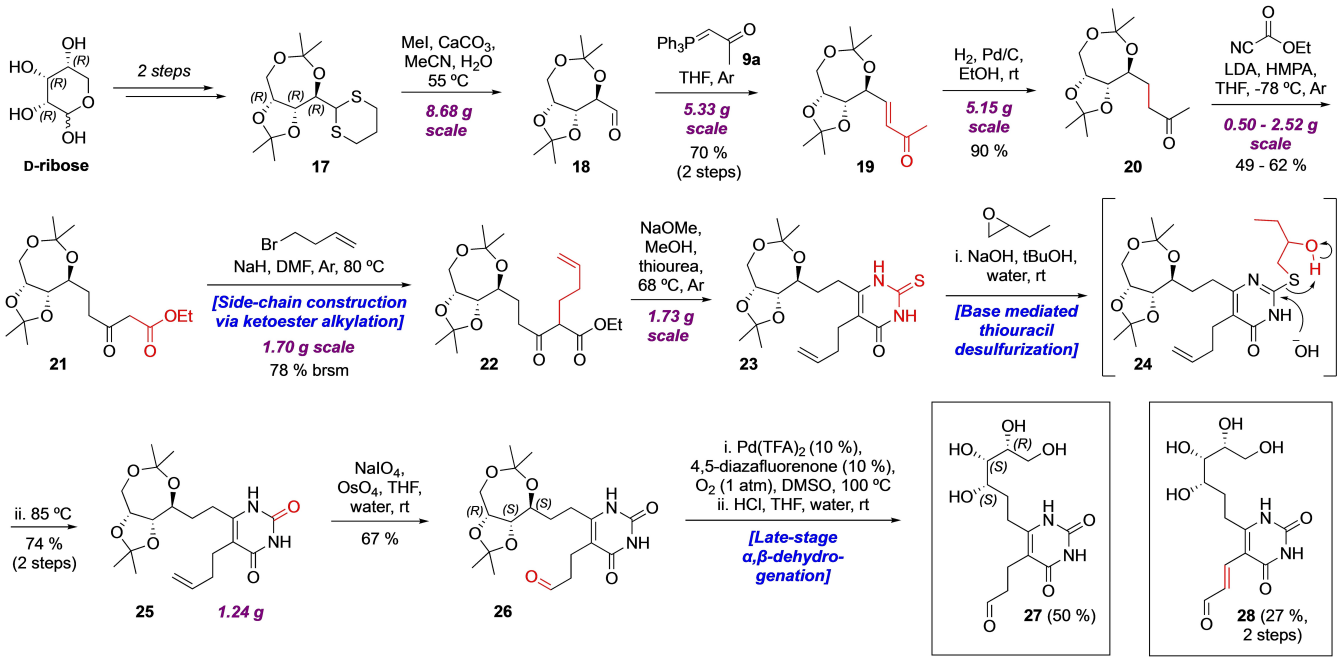

Scheme 2. Synthesis of stable analogues **27** and **28**.

A Stable, Potent Activator of MAIT cells

Since aldehyde **13** induced strong upregulation of MR1, we used it to engineer a potentially potent and stable MAIT cell activator by connecting a ribityl chain to C-6. Such compounds may become the basis for a stable new antimicrobial vaccine adjuvant.[8b] However, the yield of **13** was low, so we developed a new enal installation strategy for this molecule.

The hemiacetal of D-ribose was first opened before protecting the aldehyde and alcohols (**17**, two steps, Scheme 2). Subsequent dithiane deprotection (**18**),[26] treatment with stabilized ylide **9a** (to give **19**, 70 %, 2 steps), and hydrogenation (**20**, 90 %) proceeded in high yields. Chemoselective *C*-homologation with Mander's reagent[27] gave ketoester alkylation substrate **21**. We previously observed ribityl chelation of lithiated bases, so the enal side-chain precursor was installed with NaH and 4-bromobut-1-ene to give **22** (78 % yield based on recovered starting material).

This synthesis of the carbon skeleton produced a hindered ketoester for cyclization with thiourea.[28] Due to its bulk (restricting cyclisation to 29–67 % in similar systems[29]), the cyclocondensation was first performed with NaOEt in ethanol under reflux, and then at 100 °C in a pressurized tube. Both conditions gave **23** (50 %), but one diastereomer of **22** remained unchanged. Thus, we switched to NaOMe in refluxing methanol; although at a lower temperature, the smaller base was more efficient in this hindered system, giving **23** in high yield. Without purification, desulfurization with 1-butene oxide[30] under basic conditions gave **25** (74 %, 2 steps). This likely proceeds via **24**, where the new Lewis acidic alcohol mediated C–S bond fission, as butyl bromide alkylated **23** but the intermediate degraded upon heating.

Next, oxidation of the congested and sensitive substrate **25** with catalytic osmium tetroxide and sodium periodate unveiled aldehyde **26** regioselectively (65 %), ready for α,β-dehydrogenation to the enal sidechain. Carbonyl dehydrogenations, either metal-free or with catalytic transition metals, are typically performed on relatively featureless or protected substrates to enable enolate formation or minimize competitive coordination to the reagent.[31] Due to relative[31–32] complexity of **26**, and dehydrogenation adjacent to the functionality-rich uracil ring having no precedent, we dehydrogenated model compound **29** (synthesized like **26** from ethyl acetoacetate) to **13** to identify suitable conditions (Table 1).

Stoichiometric oxidation of **29** with 2-iodoxybenzoic acid (IBX) and *N*-methylmorpholine *N*-oxide[33] in DMSO-d_6

Table 1: Late-stage α,β-dehydrogenation model study.

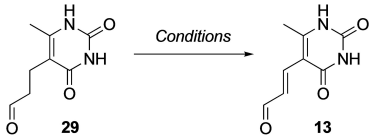

Reagents[a]	Temp.	Yield (%)
IBX (1.5 eq), NMO·H_2O (1.5 eq)	rt	3
IBX (2.2 eq), MPO·H_2O (2.2 eq)	45 °C	20
IBX (2.2 eq), DMPO·H_2O (2.2 eq)	45 °C	13
IBX (2.2 eq), MPO·H_2O (2.2 eq)[b]	rt	35
IBX (2.2 eq), DMPO·H_2O (2.2 eq)[b]	rt	36
$Pd(TFA)_2$ (10 mol %), O_2 (1 atm), 4,5-diazafluoren-9-one (10 mol %)	100 °C	45 (52[c])

[a] NMO = *N*-methylmorpholine *N*-oxide, MPO = 4-methoxypyridine *N*-oxide, DMPO = 3,4-dimethoxypyridine *N*-oxide. [b] conducted in DMSO/DCM (2:1). [c] based on recovered starting material.

gave **13** in low yields. NMR spectra suggested competitive complexation between the substrate and NMO for IBX. Switching NMO to electron-rich aromatic *N*-oxides, such as 4-methoxypyridine *N*-oxide and 3,4-dimethoxypyridine *N*-oxide (hypothesized to stabilize IBX complexes[33]) greatly improved yield (35 %).

Finally, catalytic dehydrogenation[32a] of **29** with Pd-(TFA)$_2$/4,5-diazafluorenone (10 mol %) under O_2 (1 atm) in DMSO at 100 °C consistently gave **13** in 45 % yield. These catalytic conditions were found to similarly enable dehydrogenation of **26**, although the trifluoroacetic acid generated in the catalytic cycle caused tetraol deprotection and subsequent in situ reversible dimerisation with the aldehyde. Nevertheless, same pot cleavage with aqueous acid delivered **28** in 27 % over 2 steps. Aldehyde **26** was also deprotected directly to give **27** (50 %) to test the effect of sidechain saturation on potency.

Analogues **27** and **28** were water stable (Figure S1). In inducing MR1 upregulation, aldehyde **28** was much more potent than 5-OP-RU (**4**), and 10-fold more potent than Ac-6-FP and its ketone homologue JYM72[20] (Figure 6a). Surprisingly, the saturated analogue **27** was completely inactive below 100 μM, despite its more electrophilic carbonyl and expected lower Michael acceptor capabilities, suggesting that sidechain rigidity was important for activity.

For MAIT TCR activation, we co-incubated MAIT AF7 TCR-transfected Jurkat cells (Jurkat.MAIT reporter cells)[2] and CIR.MR1 cells with test compounds and measured CD69 surface expression on the Jurkat.MAIT cells (Figure 6b, Figure S2 for individual replicates).[3] While saturated analogue **27** was similarly inactive, unsaturated aldehyde **28** was extremely potent in activating Jurkat.MAIT cells (EC_{50} 0.35 nM). It was 100-fold more potent than the ketone[20] JYM72 (EC_{50} 26 nM), and comparable to natural product 5-OP-RU (**4**) (EC_{50} 0.056 nM).

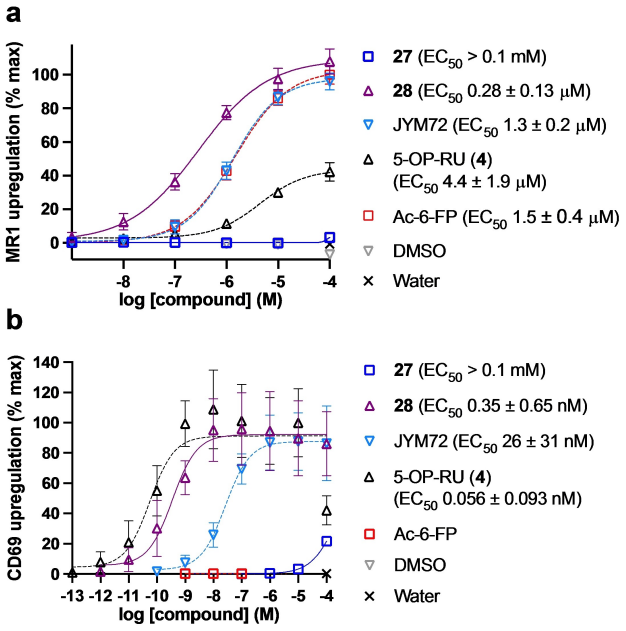

Figure 6. MR1 upregulation and MAIT cell activation by **27** and **28**. (a) Dose-dependent upregulation of MR1 surface expression on C1R.MR1 cells and (b) activation of Jurkat.MAIT cells, compared to controls (5-OP-RU (**4**), Ac-6-FP, and JYM72 (ketone homologue of **28**)). Response to 0.1 mM Ac-6-FP and 1 nM 5-OP-RU (**4**), respectively defined as 100 %. Each data point represents mean ± SEM ($n = 3$). EC_{50} values shown ± SEM.

Inhibitors of MAIT TCR Activation

Next, we asked if ligands without the ribityl chain (i.e. **10**–**16**) could competitively inhibit Jurkat.MAIT cell activation induced by 5-OP-RU (**4**) (Figure 7), using the same assay[3,34] as above, which measures surface expression of the protein CD69 upon activation of MAIT TCR-expressing Jurkat cells by 5-OP-RU (**4**) (0.1 nM). Analogues **11**, **12** and **14**–**16** had little to no inhibitory activity below 10 μM concentrations, whereas **10** (IC_{50} 900 nM) and especially **13** (IC_{50} 82 nM) both inhibited Jurkat.MAIT cell activation by 5-OP-RU (**4**). Aldehyde **13** was more potent and efficacious than any known inhibitor, including acetyl-6-formylpterin (Ac-6-FP, IC_{50} 150 nM), which only partially inhibited CD69 expression even at the highest concentration tested (100 μM).

Bimodal Ligands of MR1

Since **10** was able to bind and upregulate MR1, without the ribityl chain and with modifications to the iminocarbonyl of 5-OP-RU (**4**), we used it as an MR1-tagging motif to create other bimodal ligands. We hypothesized that diverse payloads could be linked to the C-6 position of **10** to furnish functionally distinct MR1 ligands that are chemically stable. To test this idea, we prepared an appropriately decorated uracil fragment. β-Ketoester **30** was cyclocondensed with thiourea and sodium ethoxide, and then desulfurized with chloroacetic acid and hydrochloric acid to give uracil **31**, which features a propyl-spaced carboxylic acid for payload attachment (Scheme 3). First, we attached a label that contained a diazirine, a useful precursor to a carbene for reaction with, and pulldown of, nearby proteins in cells upon UV irradiation. Attaching a minimalist diazirine-alkyne

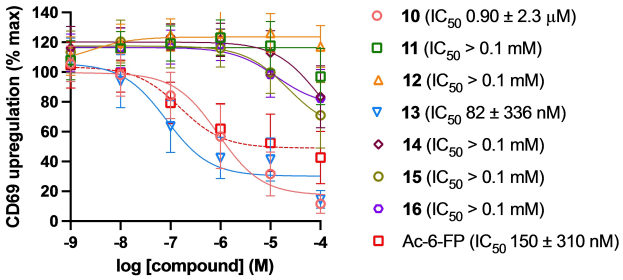

Figure 7. Inhibition by **10**–**16** of the activation of Jurkat.MAIT TRBV6-1 cells by 5-OP-RU (**4**) (0.1 nM, response defined as 100 %), relative to control Ac-6-FP. Each data point represents mean ± SEM ($n = 3$). IC_{50} values shown ± SEM.

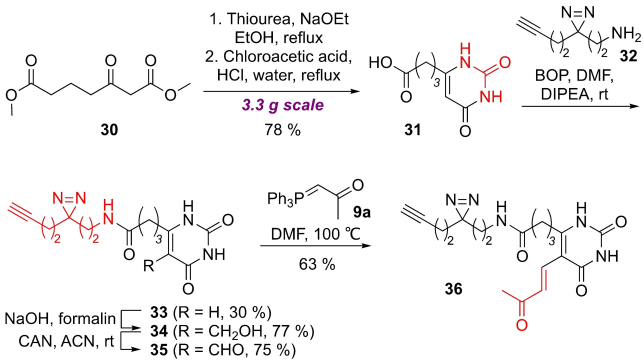

Scheme 3. Tagging MR1 ligand with a diazirine-alkyne.

label **32**[35] to **31** via amide coupling (**33**, 30 %), then hydroxymethylation (**34**, 77 %), CAN oxidation (**35**, 75 %) and Wittig elaboration gave **36** (63 %). Second, we attached biotin (to enable protein pulldown via streptavidin) or a fluorophore Cy5 or AF647 to **31** via longer linkers (Scheme 4); coupling of glycine-derived alkynyl linker **37** to give **38** (two amides to increase water solubility), enone side-chain installation (via **39**–**41**), and then cycloaddition with biotin-PEG-3 or fluorophore azides gave **42**–**44**.

We found that MR1 could be upregulated by water-stable (Figure S1) compounds **36** (EC_{50} 700 nM), **42** (EC_{50} 3.9 μM), **43** (EC_{50} 1.3 μM) and **44** (EC_{50} 6.5 μM) with potencies comparable to **4**, indicating effective cell uptake and MR1 binding despite diverse payloads (Figure 8a; Figure S3 for cell surface detection of biotin after treatment with **42**). Despite an identical MR1 binding motif, smaller compounds (e.g. **10** or **36**) promoted more potent MR1 upregulation, possibly due to better cell uptake.

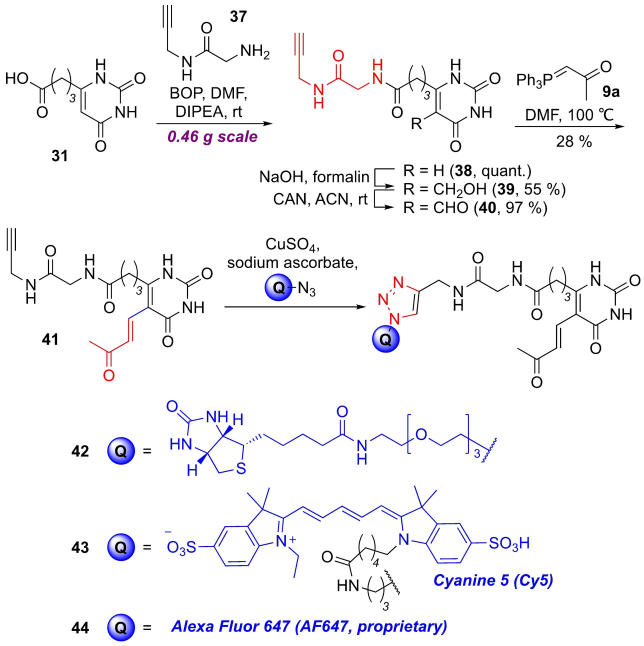

Scheme 4. Tagging MR1 ligand with biotin/fluorophore.

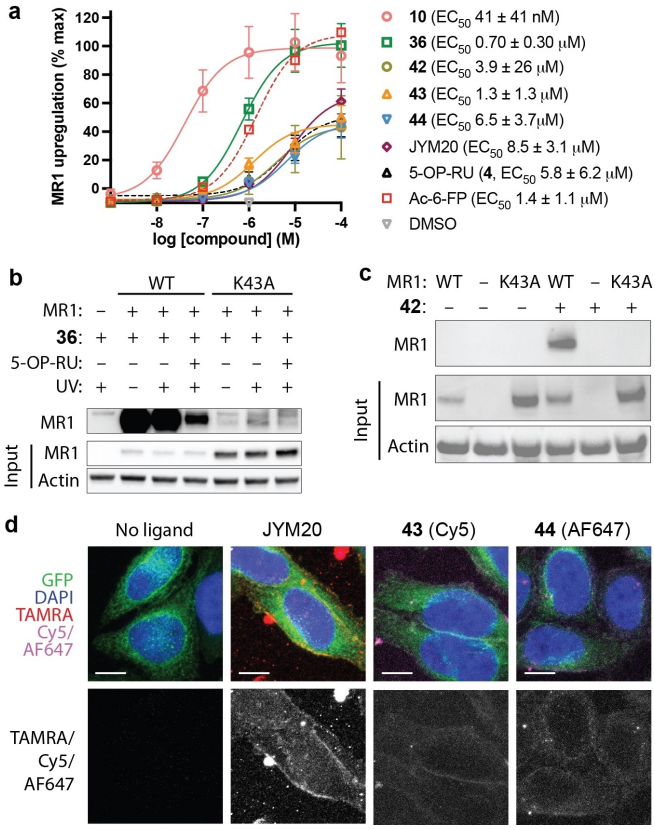

Figure 8. (a) Dose-dependent upregulation of MR1 expression on C1R.MR1 cells by **36**, **42**–**44** relative to controls 5-OP-RU (**4**), **10**, Ac-6-FP, JYM20. Response to 0.1 mM Ac-6-FP defined as 100 %. Each data point represents mean ± SEM ($n = 3$). EC_{50} values shown ± SEM. (b) Pull-down of MR1 in C1R cells using diazirine-alkyne **36** and azido-biotin reagent. See Figure S4 for full blots. (c) Streptavidin-mediated pull-down of MR1 in C1R cells with biotin-tagged **42**. See Figure S4 for full blots. (d) Binding of fluorescent **43** and **44** to MR1-GFP in HeLa.MR1-GFP cells. Scale bar = 10 μm, shown are maximum projections from Z-stacks. See Figure S6 for mean fluorescence intensity quantification.

Diazirine-alkyne analogue **36**, which can form a Schiff base with MR1, mediated pull-down of MR1 after cycloaddition with an azido-biotin in C1R cells, but not in MR1 knock-out cells (Figure 8b, lanes 1 and 2). This showed that the Schiff base formed from **36** was not completely hydrolyzed, even under conditions that promote cell lysis and protein denaturation. MR1 pulldown was mediated through specific binding, as pulldown was reduced when 5-OP-RU (**4**) was used as a competing ligand (Figure 8b, lanes 3 and 4; Figure S4).

To prove that the diazirine group could covalently link proteins, **36** was incubated with C1R cells expressing the K43A MR1 mutant. This mutant did not negatively affect MR1 folding,[6] but prevents Schiff base formation with ligand. Consequently, reduced K43A MR1 pulldown was observed relative to WT MR1 (Figure 8b, lanes 2 and 5). However, increased biotin pulldown of K43A MR1 was observed upon UV irradiation, likely via a diazirine-derived carbene, which formed a new covalent bond with MR1

(Figure 8b lanes 5 and 6, Figure S4). This was similarly outcompeted by 5-OP-RU (**4**), confirming that **36** was bound at the 5-OP-RU binding site, and that this binding did not affect the function of the diazirine-alkyne (Figure 8b, lanes 6 and 7).

Similarly, immobilized streptavidin-mediated pulldown of biotinylated analogue **42** bound to wild-type MR1 but not the K43A mutant, indicating similar MR1 binding to 5-OP-RU (**4**) (Figure 8c). Ligands tagged with fluorophore Cy5 (**43**) or AF647 (**44**) exhibited comparable cell uptake kinetics (Figure S5) and intracellular MR1-GFP binding patterns (Figure 8d, Figure S6). These compounds were functionally comparable to a TAMRA-tagged ligand that we previously used to demonstrate[36] MR1-ligand binding in the endoplasmic reticulum (JYM20, Figure 8d).

Computer Modelling

To understand how analogue modifications affected MR1 upregulation and MAIT cell activation, we calculated the ability of **10**, **13**–**16** and **29** to form non-covalent and covalent interactions in the gas phase (Figure S7–S10). The compounds had comparable tautomeric distributions, atomic partial charges, and electrostatic surface potentials. *N*-methylation removed NH donors for hydrogen bonding with MR1 S24 and also disrupted water hydrogen bonding to the C-4 carbonyl (Scheme 1, Figure 2b). Gibbs free energies for imine formation of methylamine (a model of MR1 K43) with unsaturated and saturated aldehydes **13** and **29** were 4.5 and 3.5 kcal/mol more favorable than ketone **10**, likely due to reduced steric clash.

Molecular dynamics simulations were performed on ligand-bound MR1 complexes without K43 imine bonds (Figure 9), since mutation of K43 to charge neutral alanine alone is sufficient to upregulate MR1 without adding ligand.[6] This suggests that the ligands formed imines with K43 to different extents. While **10** and **13** bound MR1 stably throughout the simulation, all other ligands (with bulkier sp^3-hybridized groups attached to uracil) were ejected from their binding site atop Y7 within 100 ns. N3-methylated analogues **14** and **16**, unable to form a hydrogen bond to S24, were expelled within 30 ns. The uracil ring of saturated aldehyde **29** bound MR1 stably 90 % of the time (Figure 9a), but its carbonyl sidechain was much more flexible (Figure 9b). In simulations with the ligands covalently bound to K43, the uracil rings of N3-methyl analogues **14** and **16** still fluctuated greatly with respect to protein (Figure S11), suggesting that S24 engagement plays a role in Y7 binding.

These calculations suggest that while the analogues were electronically comparable, their steric variations could account for the potency differences. Analogues with uracil-adjoining sp^3 groups that clashed with MR1 S24 and/or Y7 had reduced potency, indicating their importance for MR1 binding. This is consistent with an analysis of >300 RNA-protein crystal structures showing that uracil has a high propensity for pi-interactions with tyrosine or phenylalanine (typically worth 4.8–6.0 kcal/mol).[37]

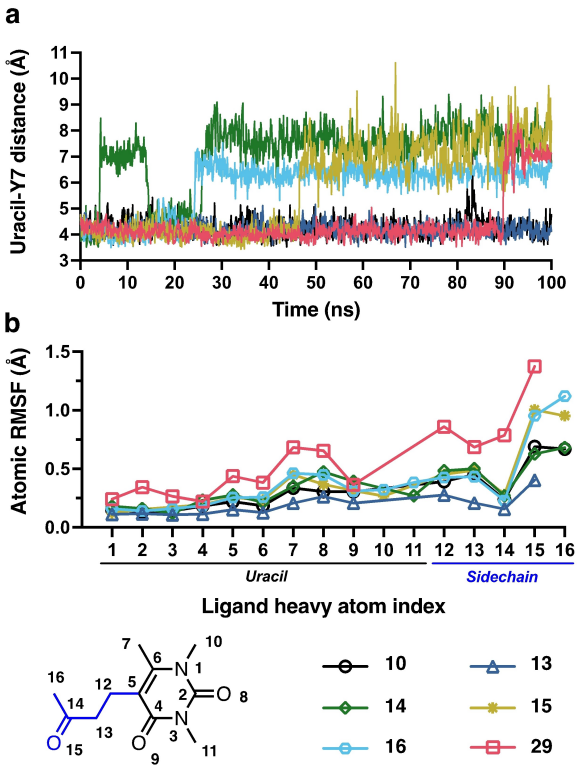

Figure 9. Molecular dynamics simulations (100 ns) of MR1 complexes of **10**, **13**–**16**, **29** without a ligand-K43 imine bond. (a) Ligand fluctuations within MR1, measured by distance between the centers of the uracil of each ligand and the phenol of Y7 in MR1. (b) Atomic root mean squared fluctuation of the 16 heavy atoms (C, N, O) in each of six MR1-bound ligands.

The most potent analogue possessed a less hindered sidechain that formed a stronger imine bond with MR1K43. This explains why enal **28** was more potent than its enone homologue JYM72 in upregulating MR1. In contrast, enal saturation (**27**), which further depleted carbonyl carbon electron density but affected Y7 engagement and increased electrophile flexibility, almost completely ablated activity. This suggests that **27** did not form an imine with MR1 K43, despite favorable sterics and electronics at the aldehyde carbon. As additions to the carbonyl carbon typically require specific nucleophile trajectories, and the limited positioning of a protein sidechain nucleophile within a ligand binding site, results are consistent with ligand-mediated MR1 refolding in which a pi-system first directs the ligand into MR1 via interactions with S24 and Y7. This orients a rigid electrophilic carbonyl group for subsequent imine formation with (and charge neutralization of) MR1 K43. This model is supported by a report of RNA-protein covalent bond formation being templated by uracil-phenylalanine pi-interactions.[38] Notably, only aromatic or unsaturated, but not aliphatic, aldehydes/ketones have been reported as MR1 ligands so far,[7,25,39] further supporting sidechain rigidity and unsaturation being important. Our new ketoester alkylation/late-stage oxidation strategy may be helpful in tuning other ligands for enhanced binding to MR1 and for validating such

a template-mediated alignment of ligands with tyrosine in MR1.

Conclusion

Motivated by the immunological importance of an unstable natural product, bacterial metabolite 5-OP-RU (**4**), in binding to MR1 protein to activate MAIT cells,[2,3] we systematically modified it to understand how structure underpins function, culminating in the development of the most potent and chemically stable MR1 ligands to date. We demonstrate that they can strongly upregulate MR1 to the cell surface, potently induce or inhibit MAIT cell activation, and importantly are much more stable than natural product **4** in water. We identified structural determinants that confer each of these properties, and key ligand-protein interactions with MR1 residues S24 and Y7 preceding covalent bonding of ligands with K43.

Compounds **10** and **13** are the most potent ligands known for upregulating MR1 expression on the cell surface. Compound **13** is ~500-fold more potent than known upregulator Ac-6-FP, under the experimental conditions used. MR1 plays an immunosurveillance role and MR1-ligand complexes can undergo ligand exchange near the cell surface.[40] Ligands that potently upregulate MR1 may help dissect mechanisms of metabolite detection and increase detection sensitivity.

Based on its superior MR1-upregulating properties, and much greater stability in water than the natural product antigen 5-OP-RU (**4**), we used **13** as a template for attaching a ribityl chain to create a water-stable potent activator of MAIT cells. Despite the potent immunostimulatory properties,[3,10a,11,20] vaccination[8b,12] and cancer therapeutic[16] potential of 5-OP-RU (**4**), its intrinsic instability and short half-life in vivo has significantly limited widespread use by the biological community and hampered determination of its true potency in vivo. Other researchers have stabilized its oxidation prone precursor 5-A-RU (**1**) as a salt[41] or prodrug,[42] but these approaches do not alter the instability of the active product 5-OP-RU (**4**). Here we overcome the stability problem, with **28** (henceforth JYM73) being the most stable potent MAIT cell activator to date. It has MAIT activating potency comparable to 5-OP-RU (**4**) and is ~100-fold more potent than ketone homologue JYM72.[20] We created this delicately functionalized enal via a robust synthesis that has enabled us to make large quantities for in vivo studies.

Compounds **10** (IC_{50} 900 nM, henceforth JYM87) and **13** (IC_{50} 82 nM, JYM88) are the most potent and most effective inhibitors of MAIT activation reported to date, both surpassing Ac-6-FP in displaying full antagonism, and coniferyl aldehyde[39] (IC_{50} 11.6 μM) in potency. MR1 deficiency or treatment with a weak inhibitor reportedly reduces oxazolone-induced colitis in mice,[19b] suggesting a therapeutic role for inhibitors of MAIT cell activation. Outcomes of infection with SARS-CoV-2 virus have also been linked to MAIT cell activation, with infected macrophages inducing MAIT cell cytotoxicity in an MR1-dependent manner.[43] Ac-6-FP has been patented as a potential treatment for dermatitis,[44] despite its poor aqueous solubility (0.4 mM), while MR1 ligand DB-28 reportedly inhibits MAIT cell activation (IC_{50} 0.09 mM) by blocking MR1 translocation to the cell surface.[45]

Finally, we attached four different payloads via different linkers to the water-stable, MR1-binding, uracil-based scaffold **10**, to create four examples of bimodal tools (**36**, **42**–**44**) for exploring MR1 immunology. We showcase applications to photoaffinity labelling with **36** (henceforth JYM31), biotin-streptavidin binding using **42** (JYM32), and fluorescence imaging with **43** (JYM21) or **44** (JYM22). These compounds highlight a more general strategy for creating bifunctional MR1 probes by appending potentially any bespoke tag that might be envisaged to explore new MR1 dependent cell biology.

Overall, these novel, functionally distinct, chemically stable, and powerful tools will be useful for characterizing MR1 and MAIT cell mediated immunology, with many potential applications. This valuable information may also inform the design of new antigens for targeting other T cells that interact with MR1 and facilitate the development of new MR1-binding therapeutics.

Supporting Information

Supplementary Figures, experimental methods, and spectral data for all new products are within the Supporting Information. The authors have cited additional references within the Supporting Information.[46]

Acknowledgements

We acknowledge grant support from University of Queensland UQECR1834385 (JYWM), Australian Research Council Centres of Excellence in Advanced Molecular Imaging CE140100011 and Innovations for Peptide and Protein Science CE200100012 (DPF), the Australian National Health and Medical Research Council of Australia for a Senior Principal fellowship 1117017 (DPF), Investigator fellowships 2009551 (DPF) and 1193745 (AJC), and an Ideas grant 2003192 (HMcW). JAV acknowledges grants from NHMRC (1113293, 1154502, 2016969) and ARC (DP170102471). AJC is supported by a Dame Kate Campbell Fellowship from University of Melbourne. JMc, JAV and DPF are supported by the US National Institutes of Health RO1 AI14807-01A1. Figure 2a was created with BioRender. Open Access publishing facilitated by The University of Queensland, as part of the Wiley - The University of Queensland agreement via the Council of Australian University Librarians.

Conflict of Interest

JYWM, AJC, JMc and DPF are among inventors on patents describing MR1 ligands and tetramers, including MAIT cell activators (e.g. compound **4**) and inhibitors.

Data Availability Statement

The data that support the findings of this study are available in the supplementary material of this article.

Keywords: Biological activity · Chemical tools · Covalent ligands · Immunology · Natural Products · Protein folding · Schiff bases

[1] N. Pishesha, T. J. Harmand, H. L. Ploegh, *Nat. Rev. Immunol.* **2022**, *22*, 751–764.
[2] L. Kjer-Nielsen, O. Patel, A. J. Corbett, J. Le Nours, B. Meehan, L. Liu, M. Bhati, Z. Chen, L. Kostenko, R. Reantragoon, N. A. Williamson, A. W. Purcell, N. L. Dudek, M. J. McConville, R. A. J. O'Hair, G. N. Khairallah, D. I. Godfrey, D. P. Fairlie, J. Rossjohn, J. McCluskey, *Nature* **2012**, *491*, 717–723.
[3] A. J. Corbett, S. B. G. Eckle, R. W. Birkinshaw, L. Liu, O. Patel, J. Mahony, Z. Chen, R. Reantragoon, B. Meehan, H. Cao, N. A. Williamson, R. A. Strugnell, D. Van Sinderen, J. Y. W. Mak, D. P. Fairlie, L. Kjer-Nielsen, J. Rossjohn, J. McCluskey, *Nature* **2014**, *509*, 361–365.
[4] E. Treiner, L. Duban, S. Bahram, M. Radosavljevic, V. Wanner, F. Tilloy, P. Affaticati, S. Gilfillan, O. Lantz, *Nature* **2003**, *422*, 164–169.
[5] D. I. Godfrey, H.-F. Koay, J. McCluskey, N. A. Gherardin, *Nat. Immunol.* **2019**, *20*, 1110–1128.
[6] H. E. G. McWilliam, S. B. G. Eckle, A. Theodossis, L. Liu, Z. Chen, J. M. Wubben, D. P. Fairlie, R. A. Strugnell, J. D. Mintern, J. McCluskey, J. Rossjohn, J. A. Villadangos, *Nat. Immunol.* **2016**, *17*, 531–537.
[7] J. Y. W. Mak, L. Liu, D. P. Fairlie, *Acc. Chem. Res.* **2021**, *54*, 3462–3475.
[8] a) A. Vacchini, A. Chancellor, J. Spagnuolo, L. Mori, G. De Libero, *Front. Immunol.* **2020**, *11*, 751; b) A. M. Downey, P. Kaplonek, P. H. Seeberger, *FEBS Lett.* **2019**, *593*, 1627–1640.
[9] a) M. D. Crowther, A. K. Sewell, *Curr. Opin. Immunol.* **2021**, *69*, 10–17; b) N. Veerapen, J. Hobrath, A. K. Besra, G. S. Besra, *Mol. Immunol.* **2021**, *129*, 114–120; c) M. D. Crowther, G. Dolton, M. Legut, M. E. Caillaud, A. Lloyd, M. Attaf, S. A. E. Galloway, C. Rius, C. P. Farrell, B. Szomolay, A. Ager, A. L. Parker, A. Fuller, M. Donia, J. McCluskey, J. Rossjohn, I. M. Svane, J. D. Phillips, A. K. Sewell, *Nat. Immunol.* **2020**, *21*, 178–185.
[10] a) F. Legoux, D. Bellet, C. Daviaud, Y. El Morr, A. Darbois, K. Niort, E. Procopio, M. Salou, J. Gilet, B. Ryffel, A. Balvay, A. Foussier, M. Sarkis, A. El Marjou, F. Schmidt, S. Rabot, O. Lantz, *Science* **2019**, *366*, 494–499; b) H. F. Koay, N. A. Gherardin, A. Enders, L. Loh, L. K. Mackay, C. F. Almeida, B. E. Russ, C. A. Nold-Petry, M. F. Nold, S. Bedoui, Z. Chen, A. J. Corbett, S. B. G. Eckle, B. Meehan, Y. d'Udekem, I. E. Konstantinov, M. Lappas, L. Liu, C. C. Goodnow, D. P. Fairlie, J. Rossjohn, M. M. Chong, K. Kedzierska, S. P. Berzins, G. T. Belz, J. McCluskey, A. P. Uldrich, D. I. Godfrey, D. G. Pellicci, *Nat. Immunol.* **2016**, *17*, 1300–1311; c) H.-F. Koay, S. Su, D. Amann-Zalcenstein, S. R. Daley, I. Comerford, L. Miosge, C. E. Whyte, I. E. Konstantinov, Y. d'Udekem, T. Baldwin, P. F. Hickey, S. P. Berzins, J. Y. W. Mak, Y. Sontani, C. M. Roots, T. Sidwell, A. Kallies, Z. Chen, S. Nüssing, K. Kedzierska, L. K. Mackay, S. R. McColl, E. K. Deenick, D. P. Fairlie, J. McCluskey, C. C. Goodnow, M. E. Ritchie, G. T. Belz, S. H. Naik, D. G. Pellicci, D. I. Godfrey, *Sci. Immunol.* **2019**, *4*, eaay6039.
[11] M. G. Constantinides, V. M. Link, S. Tamoutounour, A. C. Wong, P. J. Perez-Chaparro, S.-J. Han, Y. E. Chen, K. Li, S. Farhat, A. Weckel, S. R. Krishnamurthy, I. Vujkovic-Cvijin, J. L. Linehan, N. Bouladoux, E. D. Merrill, S. Roy, D. J. Cua, E. J. Adams, A. Bhandoola, T. C. Scharschmidt, J. Aubé, M. A. Fischbach, Y. Belkaid, *Science* **2019**, *366*, eaax6624.
[12] a) H. Wang, C. D'Souza, X. Y. Lim, L. Kostenko, T. J. Pediongco, S. B. G. Eckle, B. S. Meehan, M. Shi, N. Wang, S. Li, L. Liu, J. Y. W. Mak, D. P. Fairlie, Y. Iwakura, J. M. Gunnersen, A. W. Stent, D. I. Godfrey, J. Rossjohn, G. P. Westall, L. Kjer-Nielsen, R. A. Strugnell, J. McCluskey, A. J. Corbett, T. S. C. Hinks, Z. Chen, *Nat. Commun.* **2018**, *9*, 3350; b) H. Wang, L. Kjer-Nielsen, M. Shi, C. D'Souza, T. Pediongco, H. Cao, L. Kostenko, X. Y. Lim, S. B. G. Eckle, B. S. Meehan, T. Zhu, B. Wang, Z. Zhao, J. Y. W. Mak, D. P. Fairlie, M. W. L. Teng, J. Rossjohn, D. Yu, B. Fazekas de St Groth, G. Lovrecz, L. Lu, J. McCluskey, R. Strugnell, A. J. Corbett, Z. Chen, *Sci. Immunol.* **2019**, *4*, eaaw0402.
[13] S. Sakai, K. D. Kauffman, S. Oh, C. E. Nelson, C. E. Barry III, D. L. Barber, *Mucosal Immunol.* **2021**, *14*, 199–208.
[14] T. S. C. Hinks, E. Marchi, M. Jabeen, M. Olshansky, A. Kurioka, T. J. Pediongco, B. S. Meehan, L. Kostenko, S. J. Turner, A. J. Corbett, Z. Chen, P. Klenerman, J. McCluskey, *Cell Rep.* **2019**, *28*, 3249–3262.
[15] N. A. Gherardin, L. Loh, L. Admojo, A. J. Davenport, K. Richardson, A. Rogers, P. K. Darcy, M. R. Jenkins, H. M. Prince, S. J. Harrison, H. Quach, D. P. Fairlie, K. Kedzierska, J. McCluskey, A. P. Uldrich, P. J. Neeson, D. S. Ritchie, D. I. Godfrey, *Sci. Rep.* **2018**, *8*, 4159.
[16] E. V. Petley, H.-F. Koay, M. A. Henderson, K. Sek, K. L. Todd, S. P. Keam, J. Lai, I. G. House, J. Li, M. Zethoven, A. X. Y. Chen, A. J. Oliver, J. Michie, A. J. Freeman, L. Giuffrida, J. D. Chan, A. Pizzolla, J. Y. W. Mak, T. R. McCulloch, F. Souza-Fonseca-Guimaraes, C. J. Kearney, R. Millen, R. G. Ramsay, N. D. Huntington, J. McCluskey, J. Oliaro, D. P. Fairlie, P. J. Neeson, D. I. Godfrey, P. A. Beavis, P. K. Darcy, *Nat. Commun.* **2021**, *12*, 4746.
[17] C. D'Souza, T. Pediongco, H. Wang, J.-P. Y. Scheerlinck, L. Kostenko, R. Esterbauer, A. W. Stent, S. B. G. Eckle, B. S. Meehan, R. A. Strugnell, H. Cao, L. Liu, J. Y. W. Mak, G. Lovrecz, L. Lu, D. P. Fairlie, J. Rossjohn, J. McCluskey, A. L. Every, Z. Chen, A. J. Corbett, *J. Immunol.* **2018**, *200*, 1901–1916.
[18] G. Lezmi, R. Abou-Taam, N. Garcelon, C. Dietrich, F. Machavoine, C. Delacourt, K. Adel-Patient, M. Leite-de-Moraes, *J. Allergy Clin. Immunol.* **2019**, *144*, 1714–1716.e6.
[19] a) N. E. Serriari, M. Eoche, L. Lamotte, J. Lion, M. Fumery, P. Marcelo, D. Chatelain, A. Barre, E. Nguyen-Khac, O. Lantz, J. L. Dupas, E. Treiner, *Clin. Exp. Immunol.* **2014**, *176*, 266–274; b) Y. Yasutomi, A. Chiba, K. Haga, G. Murayama, A. Makiyama, T. Kuga, M. Watanabe, R. Okamoto, A. Nagahara, T. Nagaishi, S. Miyake, *Cell. Mol. Gastroenterol. Hepatol.* **2022**, *13*, 81–93.
[20] J. Y. W. Mak, W. Xu, R. C. Reid, A. J. Corbett, B. S. Meehan, H. Wang, Z. Chen, J. Rossjohn, J. McCluskey, L. Liu, D. P. Fairlie, *Nat. Commun.* **2017**, *8*, 14599.
[21] a) G. J. M. Ler, W. Xu, J. Y. W. Mak, L. Liu, P. V. Bernhardt, D. P. Fairlie, *Chem. Eur. J.* **2019**, *25*, 15594–15608; b) W. Awad, G. J. M. Ler, W. Xu, A. N. Keller, J. Y. W. Mak, X. Y. Lim, L. Liu, S. B. G. Eckle, J. Le Nours, J. McCluskey, D. P. Fairlie, J. Rossjohn, *Nat. Immunol.* **2020**, *21*, 400–411; c) C. D.

Braganza, C. Motozono, K.-H. Sonoda, S. Yamasaki, K. Shibata, M. S. M. Timmer, B. L. Stocker, *Chem. Commun.* **2020**, *56*, 5291–5294; d) T. Matsuoka, C. Motozono, A. Hattori, H. Kakeya, S. Yamasaki, S. Oishi, H. Ohno, S. Inuki, *ChemBioChem* **2021**, *22*, 672–678.
[22] D. R. Hwang, P. Helquist, M. S. Shekhani, *J. Org. Chem.* **1985**, *50*, 1264–1271.
[23] M. Botta, M. Cavalieri, D. Ceci, F. De Angelis, G. Finizia, R. Nicoletti, *Tetrahedron* **1984**, *40*, 3313–3320.
[24] R. J. Mayer, A. R. Ofial, *Angew. Chem. Int. Ed.* **2019**, *58*, 17704–17708.
[25] A. N. Keller, S. B. G. Eckle, W. Xu, L. Liu, V. A. Hughes, J. Y. W. Mak, B. S. Meehan, T. Pediongco, R. W. Birkinshaw, Z. Chen, H. Wang, C. D'Souza, L. Kjer-Nielsen, N. A. Gherardin, D. I. Godfrey, L. Kostenko, A. J. Corbett, A. W. Purcell, D. P. Fairlie, J. McCluskey, J. Rossjohn, *Nat. Immunol.* **2017**, *18*, 402–411.
[26] P. Allevi, P. Ciuffreda, G. Tarocco, M. Anastasia, *Tetrahedron: Asymmetry* **1995**, *6*, 2357–2364.
[27] L. N. Mander, S. P. Sethi, *Tetrahedron Lett.* **1983**, *24*, 5425–5428.
[28] P. Crepaldi, B. Cacciari, M.-C. Bonache, G. Spalluto, K. Varani, P. A. Borea, I. von Kuegelgen, K. Hoffmann, M. Pugliano, C. Razzari, M. Cattaneo, *Bioorg. Med. Chem.* **2009**, *17*, 4612–4621.
[29] a) I. M. Tkachenko, V. B. Rybakov, Y. N. Klimochkin, *Synthesis* **2019**, *51*, 1482–1490; b) D. Rotili, V. Carafa, D. Tarantino, G. Botta, A. Nebbioso, L. Altucci, A. Mai, *Bioorg. Med. Chem.* **2011**, *19*, 3659–3668.
[30] I. A. Novakov, B. S. Orlinson, M. B. Navrotskii, *Russ. J. Org. Chem.* **2005**, *41*, 607–609.
[31] H. Chen, L. Liu, T. Huang, J. Chen, T. Chen, *Adv. Synth. Catal.* **2020**, *362*, 3332–3346.
[32] a) T. Diao, T. J. Wadzinski, S. S. Stahl, *Chem. Sci.* **2012**, *3*, 887–891; b) S. Gnaim, J. C. Vantourout, F. Serpier, P.-G. Echeverria, P. S. Baran, *ACS Catal.* **2021**, *11*, 883–892.
[33] K. C. Nicolaou, T. Montagnon, P. S. Baran, *Angew. Chem. Int. Ed.* **2002**, *41*, 993–996.
[34] S. B. G. Eckle, R. W. Birkinshaw, L. Kostenko, A. J. Corbett, H. E. G. McWilliam, R. Reantragoon, Z. Chen, N. A. Gherardin, T. Beddoe, L. Liu, O. Patel, B. Meehan, D. P. Fairlie, J. A. Villadangos, D. I. Godfrey, L. Kjer-Nielsen, J. McCluskey, J. Rossjohn, *J. Exp. Med.* **2014**, *211*, 1585–1600.
[35] Z. Li, P. Hao, L. Li, C. Y. J. Tan, X. Cheng, G. Y. J. Chen, S. K. Sze, H.-M. Shen, S. Q. Yao, *Angew. Chem. Int. Ed.* **2013**, *52*, 8551–8556.
[36] H. E. G. McWilliam, J. Y. W. Mak, W. Awad, M. Zorkau, S. Cruz-Gomez, H. J. Lim, Y. Yan, S. Wormald, L. F. Dagley, S. B. G. Eckle, A. J. Corbett, H. Liu, S. Li, S. J. J. Reddiex, J. D. Mintern, L. Liu, J. McCluskey, J. Rossjohn, D. P. Fairlie, J. A. Villadangos, *Proc. Natl. Acad. Sci. USA* **2020**, *117*, 24974–24985.
[37] K. A. Wilson, R. W. Kung, S. D'souza, S. D. Wetmore, *Nucleic Acids Res.* **2021**, *49*, 2213–2225.
[38] A. Knörlein, C. P. Sarnowski, T. de Vries, M. Stoltz, M. Götze, R. Aebersold, F. H.-T. Allain, A. Leitner, J. Hall, *Nat. Commun.* **2022**, *13*, 2719.
[39] T. Matsuoka, A. Hattori, S. Oishi, M. Araki, B. Ma, T. Fujii, N. Arichi, Y. Okuno, H. Kakeya, S. Yamasaki, H. Ohno, S. Inuki, *J. Med. Chem.* **2023**, *66*, 12520–12535.
[40] C. Kulicke, E. Karamooz, D. Lewinsohn, M. Harriff, *Front. Immunol.* **2020**, *11*, 2034.
[41] K. Li, C. K. Vorkas, A. Chaudhry, D. L. Bell, R. A. Willis, A. Rudensky, J. D. Altman, M. S. Glickman, J. Aubé, *PLoS One* **2018**, *13*, e0191837.
[42] J. Lange, R. J. Anderson, A. J. Marshall, S. T. S. Chan, T. S. Bilbrough, O. Gasser, C. Gonzalez-Lopez, M. Salio, V. Cerundolo, I. F. Hermans, G. F. Painter, *ACS Chem. Biol.* **2020**, *15*, 437–445.
[43] H. Flament, M. Rouland, L. Beaudoin, A. Toubal, L. Bertrand, S. Lebourgeois, C. Rousseau, P. Soulard, Z. Gouda, L. Cagninacci, A. C. Monteiro, M. Hurtado-Nedelec, S. Luce, K. Bailly, M. Andrieu, B. Saintpierre, F. Letourneur, Y. Jouan, M. Si-Tahar, T. Baranek, C. Paget, C. Boitard, A. Vallet-Pichard, J.-F. Gautier, N. Ajzenberg, B. Terrier, F. Pène, J. Ghosn, X. Lescure, Y. Yazdanpanah, B. Visseaux, D. Descamps, J.-F. Timsit, R. C. Monteiro, A. Lehuen, *Nat. Immunol.* **2021**, *22*, 322–335.
[44] a) O. Gasser, K. Parata, K. Naidoo, WO 2020/080957 A1, **2020**; b) K. Naidoo, K. Woods, C. Pellefigues, A. Cait, D. O'Sullivan, K. Gell, A. J. Marshall, R. J. Anderson, Y. Li, A. Schmidt, K. Prasit, J. U. Mayer, A. Gestin, I. F. Hermans, G. Painter, E. A. Jacobsen, O. Gasser, *Allergy* **2021**, *76*, 3155–3170.
[45] M. Salio, W. Awad, N. Veerapen, C. Gonzalez-Lopez, C. Kulicke, D. Waithe, A. W. J. Martens, D. M. Lewinsohn, J. V. Hobrath, L. R. Cox, J. Rossjohn, G. S. Besra, V. Cerundolo, *Proc. Natl. Acad. Sci. USA* **2020**, *117*, 10465–10475.
[46] a) T. W. Schultz, J. W. Yarbrough, E. L. Johnson, *SAR QSAR Environ. Res.* **2005**, *16*, 313–322; b) D. Mulliner, D. Wondrousch, G. Schüürmann, *Org. Biomol. Chem.* **2011**, *9*, 8400–8412; c) J. Y. W. Mak, *Aust. J. Chem.* **2022**, *75*, 160–164; d) G. Wider, L. Dreier, *J. Am. Chem. Soc.* **2006**, *128*, 2571–2576; e) H. Kuroda, E. Hanaki, H. Izawa, M. Kano, H. Itahashi, *Tetrahedron* **2004**, *60*, 1913–1920; f) R. M. Williams, B. H. Lee, M. M. Miller, O. P. Anderson, *J. Am. Chem. Soc.* **1989**, *111*, 1073–1081.

Manuscript received: January 10, 2024
Accepted manuscript online: April 28, 2024
Version of record online: June 26, 2024